ENVIRONMENTAL RESEARCH
LETTERS

LETTER • OPEN ACCESS

A brown wave of riparian woodland mortality following groundwater declines during the 2012–2019 California drought

ENVIRONMENTAL RESEARCH
LETTERS

OPEN ACCESS

RECEIVED
5 May 2021

REVISED
17 June 2021

ACCEPTED FOR PUBLICATION
12 July 2021

PUBLISHED
28 July 2021

LETTER

A brown wave of riparian woodland mortality following groundwater declines during the 2012–2019 California drought

Christopher L Kibler[1], E Claire Schmidt[2], Dar A Roberts[1,3], John C Stella[4], Li Kui[3,5], Adam M Lambert[5,6] and Michael Bliss Singer[3,7,8]

[1] Department of Geography, University of California, Santa Barbara, CA 93106, United States of America
[2] Department of Biology, Knox College, Galesburg, IL 61401, United States of America
[3] Earth Research Institute, University of California, Santa Barbara, CA 93106, United States of America
[4] Department of Sustainable Resources Management, State University of New York College of Environmental Science and Forestry, Syracuse, NY 13210, United States of America
[5] Marine Science Institute, University of California, Santa Barbara, CA 93106, United States of America
[6] Cheadle Center for Biodiversity and Ecological Restoration, University of California, Santa Barbara, CA 93106, United States of America
[7] School of Earth and Environmental Sciences, Cardiff University, CF10 3AT Cardiff, United Kingdom
[8] Water Research Institute, Cardiff University, Cardiff CF10 3AX, United Kingdom

E-mail: kibler@ucsb.edu

Keywords: riparian, remote sensing, drought, forest die-off, phreatophyte, groundwater dependent ecosystem, California

Supplementary material for this article is available online

Abstract

As droughts become more frequent and more severe under anthropogenic climate change, water stress due to diminished subsurface supplies may threaten the health and function of semi-arid riparian woodlands, which are assumed to be largely groundwater dependent. To better support the management of riparian woodlands under changing climatic conditions, it is essential to understand the sensitivity of riparian woodlands to depth to groundwater (DTG) across space and time. In this study, we examined six stands of riparian woodland along 28 km of the Santa Clara River in southern California. Combining remote sensing data of fractional land cover, based on spectral mixture analysis, with historical groundwater data, we assessed changes in riparian woodland health in response to DTG during the unprecedented 2012–2019 California drought. We observed a coherent 'brown wave' of tree mortality, characterized by decreases in healthy vegetation cover and increases in dead/woody vegetation cover, which progressed downstream through the Santa Clara River corridor between 2012 and 2016. We also found consistent, significant relationships between DTG and healthy vegetation cover, and separately between DTG and dead/woody vegetation cover, indicating that woodland health deteriorated in a predictable fashion as the water table declined at different sites and different times. Based on these findings, we conclude that the brown wave of vegetation dieback was likely caused by local changes in DTG associated with the propagation of precipitation deficits into a depleted shallow alluvial aquifer. These factors suggest that semi-arid riparian woodlands are strongly dependent on shallow groundwater availability, which is in turn sensitive to climate forcing.

1. Introduction

Riparian trees often rely on shallow groundwater to meet their water needs, so water table declines during increasingly frequent and severe drought conditions threaten the health and function of riparian woodlands (Diffenbaugh *et al* 2015, Meixner *et al* 2016, Rohde *et al* 2017, Williams *et al* 2020). Though many studies have examined the sensitivity of individual species to drought and local groundwater availability (e.g. Stromberg *et al* 1996, Singer *et al* 2014, Sargeant and Singer 2016, Pettit and Froend 2018, Skiadaresis *et al* 2021), few studies have considered the landscape-scale responses of riparian woodlands to drought across space and time, and even fewer in relation to direct groundwater measurements (but see Rohde *et al* 2021). These knowledge gaps are relevant to dryland watersheds around the globe, where

convergent pressures on water resources from agriculture, urban development, and climate change are increasing (Taylor *et al* 2013, Rohde *et al* 2017, Rateb *et al* 2020).

Riparian woodlands are ecologically important plant communities that provide habitat for sensitive animal species (Kus 1998, Merritt and Bateman 2012, Bateman and Merritt 2020), promote plant biodiversity (Stromberg *et al* 1996, Stromberg and Merritt 2016), and contain a disproportionately large amount of the biomass in dryland watersheds (Swetnam *et al* 2017, Matzek *et al* 2018, Dybala *et al* 2019). They form in convergent topographic zones, which serve as hydrologic refugia and are somewhat buffered from normal climatic variability (Brooks *et al* 2015, Hoylman *et al* 2019). Riparian tree species are typically phreatophytes, which have taproot systems that extend up to 5 m down to the capillary fringe above perennial water tables (Stromberg 2013, Rohde *et al* 2017). Phreatophytes are extremely sensitive to water availability at all life stages (Mahoney and Rood 1998, Stella and Battles 2010, Singer *et al* 2013). If their root systems lose contact with the alluvial water table, phreatophytes commonly exhibit stomatal closure, leaf abscission, branch dieback, and xylem cavitation (Scott *et al* 1999, Leffler *et al* 2000, Rood *et al* 2000). Prolonged water table declines, for example during extreme drought conditions, can lead to whole-plant mortality if a tree's hydraulic system cannot maintain a favorable water balance as groundwater supply declines (Scott *et al* 1999, Cooper *et al* 2003).

From 2012 to 2019, California experienced the most severe drought in its paleoclimate record (Robeson 2015). Meteorological drought conditions first emerged in northern California around January 2012 and then spread southward (U.S. Drought Monitor 2021). The meteorological drought propagated into hydrological (van Loon 2015) and ecological (Kovach *et al* 2019, Munson *et al* 2020) droughts in dryland regions throughout southern California (Okin *et al* 2018, Dong *et al* 2019, Warter *et al* 2021). Record low precipitation and record high temperatures (Diffenbaugh *et al* 2015) substantially reduced soil moisture (Warter *et al* 2021), streamflow (Konrad 2019), groundwater storage (Thomas *et al* 2017), and upland canopy water content (Asner *et al* 2016) throughout the region. While the drought is known to have generated mass die-off of upland trees (e.g. Goulden and Bales 2019), there is a notable lack of quantitative assessments of drought-induced mortality of lowland riparian phreatophytes, particularly within dryland regions. Documenting large-scale ecological die-offs, particularly in ecosystems that are buffered from climate impacts by their hydrogeomorphic setting, is important for identifying global signals of forests being pushed past their tolerance for environmental change (Allen *et al* 2010, 2015, Anderegg *et al* 2013, McDowell *et al* 2016).

Remote sensing is a powerful tool for analyzing the sensitivity of vegetation health to changes in the water availability, but few remote sensing studies have quantified the sensitivity of groundwater-dependent ecosystems to water table declines (e.g. Barron *et al* 2014, Huntington *et al* 2016). In this study, we combined time series remote sensing imagery with data from groundwater monitoring wells to investigate the fate and trajectory of riparian woodlands in southern California during the unprecedented 2012–2019 California drought. We used spectral mixture analysis (SMA) to discriminate between healthy and dead vegetation cover in remote sensing imagery. We then analyzed the relationship between vegetation cover and depth to groundwater (DTG) in a range of woodland stands that represent a gradient of groundwater availability. These data enabled us to characterize the trajectory and the spatial progression of drought impacts across an ecologically and economically important river corridor, and to monitor the initial drought recovery in the riparian woodlands.

2. Methods

2.1. Study area

The Santa Clara River flows 132 km from the Mojave Desert to the Pacific Ocean and has a catchment covering 4200 km^2 in Ventura and Los Angeles Counties, California (Beller *et al* 2016). Mean annual precipitation ranges from 200 to 800 mm, with the wettest regions at high elevations (catchment relief 2700 m) and near the coast (Downs *et al* 2013). The basin has a Mediterranean climate with cool, wet winters and warm, dry summers, and many reaches of the Santa Clara River are ephemeral (i.e. flowing only part of most years). Winter rainfall produces flashy flows, and more than half of the annual discharge occurs during a small number of precipitation events (Downs *et al* 2013, Beller *et al* 2016). The river corridor has been subject to extensive urban and agricultural development over the last century, but the main stem of the river has not been severely controlled by engineering structures, making it the largest river in southern California that is mostly free flowing (Downs *et al* 2013, Beller *et al* 2016).

The native riparian woodlands along the Santa Clara River are discontinuous, existing at locations where groundwater is close to the surface under normal conditions (Beller *et al* 2016). The riparian woodlands are dominated by phreatophytic tree and shrub species, including *Populus fremontii, Populus trichocarpa, Salix laevigata, Salix lasiolepis*, and *Salix exigua*. The roots for these species are typically concentrated in the top 2 m of the soil profile (table 1; The Nature Conservancy 2021), although phreatophytes exhibit a considerable degree of plasticity in rooting depth in response to local groundwater conditions (Shafroth *et al* 2000, Rood *et al* 2011).

Table 1. Rooting depths for tree and shrub species that are prevalent in riparian woodlands in the Santa Clara River floodplain.

Species	Rooting depth (m)	Source
Populus fremontii	1.4 (max)	Shafroth *et al* (2000)[a]
Populus fremontii	2.1+ (max)	Zimmerman (1969)
Populus fremontii	0.8 (max)	Rood *et al* (2011)
Populus trichocarpa	0.65 (max)	Rood *et al* (2011)
Salix laevigata	1+ (max)	Stover *et al* (2018)
Salix exigua	0.51 (min)	U.S. Department of Agriculture (2021)
Baccharis salicifolia	0.3 (min)	U.S. Department of Agriculture (2021)
Baccharis salicifolia	0.6 (max)	Gary (1963), Stromberg (2013)

[a] Study that measured three-year-old saplings.

2.2. Study sites

We identified six stands of *Populus-Salix* riparian woodlands in the lower Santa Clara River floodplain that are thought to be supported by perennial shallow aquifers (figure 1; Beller *et al* 2016). The woodlands range in area from 7 to 120 ha, and they represent the most substantial woodlands that were present before the 2012–2019 drought (Beller *et al* 2016). The study sites are distinguished by transitions in hydrology or river management that facilitate shallow groundwater depths. Site boundaries were manually digitized in GIS software using 2012 aerial imagery acquired by the National Agricultural Imagery Program (U.S. Department of Agriculture 2012).

2.3. Depth to groundwater

We calculated DTG at each of the study sites using measurements from nearby wells acquired from the California Department of Water Resources (https://sgma.water.ca.gov/webgis/?appid=SGMADataViewer), United Water Conservation District, and the County of Ventura. We also used unpublished data from shallow monitoring wells that were installed by members of our team at two of the study sites (tables S1, S2; figures S1–S4 (available online at stacks.iop.org/ERL/16/084030/mmedia)). The shallow wells are ∼3 m deep and were installed between 2015 and 2020. They are manually measured twice per month. We used two different protocols to calculate DTG at the study sites, depending on the well data availability for each site (see supplementary material).

2.4. Remote sensing data acquisition and processing

SMA was used to map the fractional cover of green vegetation (GV), non-photosynthetic vegetation (NPV; i.e. dead and woody plant material), and soil in the Santa Clara River floodplain (Smith *et al* 1990, Roberts *et al* 1998). The SMA model was calibrated using data from the Airborne Visible/Infrared Imaging Spectrometer (Green *et al* 1998) and *in situ* spectra (see supplementary material). We analyzed Landsat images (spatial resolution of 30 m) acquired every June between 2011 and 2018. The June 2011 image provides a pre-drought baseline (U.S. Drought Monitor 2021). The June 2012–2018 images capture all of the growing seasons during the drought. Data from 2012 were omitted because of the scan line corrector failure on Landsat 7 (Markham *et al* 2004). The SMA model generated estimates of the fractional cover of GV, NPV, and soil within each pixel for each image. While the SMA method did not classify species cover, qualitative observations of species cover were made during field visits to the sites between 2017 and 2021, and by manually examining high resolution aerial imagery captured before, during, and after the drought.

2.5. Analysis of drought effects on vegetation

The fractional cover data and the groundwater data were used to conduct two analyses. First, the GV and NPV fractions were used to examine the spatial and temporal trends of woodland mortality along the river corridor. Mortality was indicated by a decrease in GV fractions and an increase in NPV fractions (Huang *et al* 2019). Significant differences in land cover fractions for each study site across time were identified using a Kruskal–Wallis test and a post-hoc Dunn's test with a Holm adjustment ($\alpha = 0.05$).

Second, we quantified the sensitivity of GV and NPV fractions to DTG. The median GV and NPV fractions were calculated for each study site and each year. We used the DTG measurements that were closest in time to the Landsat image acquisition dates. The difference between the well measurement dates and the image acquisition dates ranged from 0 day to 36 days with a median of 13 days. The sensitivity analyses were divided into two distinct time spans. The first time span was limited to data from 2011 to 2016, representing the period when the drought became progressively more severe, as evidenced by increasing DTG, below-average soil moisture (Warter *et al* 2021), and decreasing Standardized Precipitation Evaporation Index (SPEI). The 2011–2016 observations were pooled across sites and years, and mixed effect logistic-binomial regression (Gelman and Hill 2007) was used to determine if DTG is a significant predictor of GV and NPV fractions. Site was included as a random effect in the models to account for local

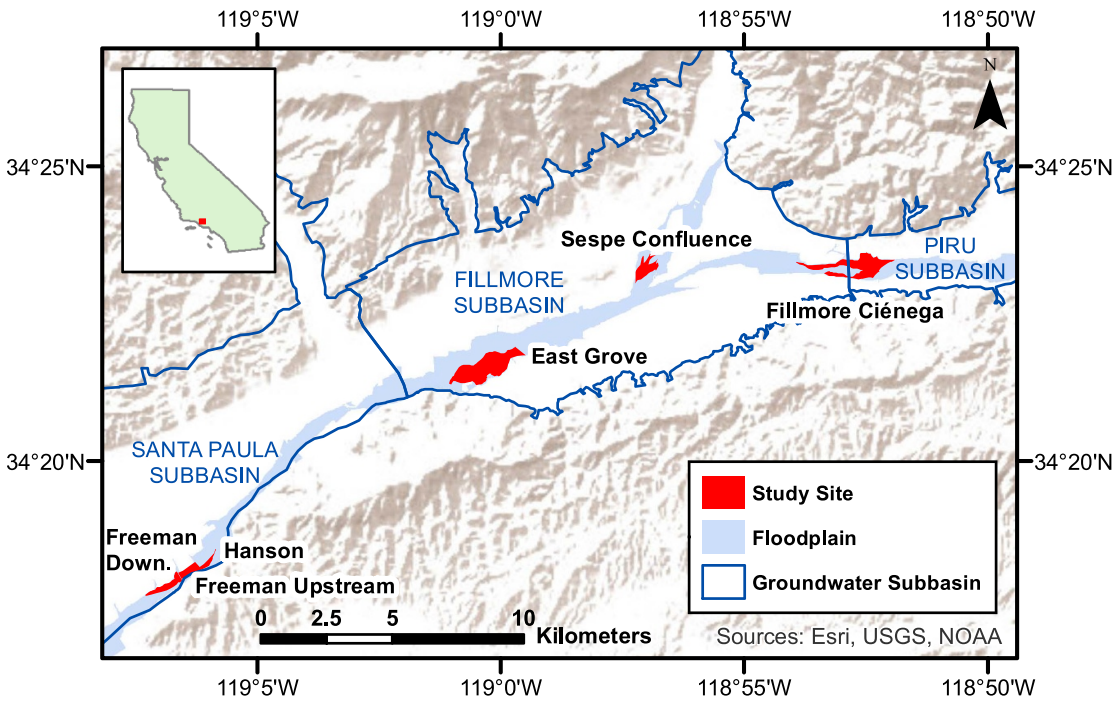

Figure 1. Location of the study sites in the floodplain of the Santa Clara River, California, USA. The river flows from east to west.

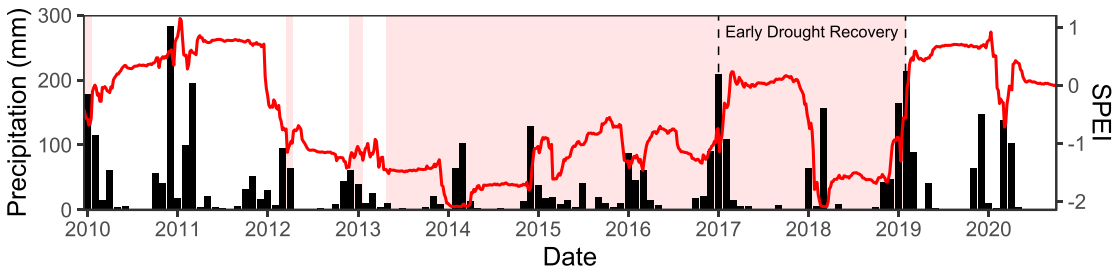

Figure 2. Mean monthly precipitation (black bars) and 12 month Standardized Precipitation Evaporation Index (SPEI; red line) in the Santa Clara River watershed (Abatzoglou 2013, Huntington *et al* 2017). The red shading indicates periods of drought according to the U.S. Drought Monitor (2021). The date labels indicate 1 January of each year.

influences on the vegetation unrelated to groundwater (see supplementary material).

The second time span was limited to data from 2017 and 2018, which represents a period of early drought recovery in the riparian woodlands. Substantial rainfall in the winter of 2016–2017 reduced DTG and increased soil moisture in the region (Warter *et al* 2021). As a result, the ecological drought began to subside, even though meteorological drought conditions persisted until 2019. The sensitivity of an ecological response to an environmental driver often differs based on the direction of the change. Differing sensitivities during decline and recovery phases can result in hysteresis in ecological systems (Beisner *et al* 2003, Andersen *et al* 2009). The 2017–2018 data were used to determine if there were differences in the sensitivity to DTG during the early stages of drought recovery as compared to the drought onset years of 2011–2016. The observed land cover fractions from 2017 and 2018 were compared to the values predicted by the regression model that was calibrated using data from 2011 to 2016. This indicated whether sensitivity to DTG differed during the two phases. Mean absolute error (MAE) was used to quantify the difference between the observed and predicted values during the two phases.

3. Results

3.1. Drought timeline

The Santa Clara River watershed experienced moderate drought conditions throughout much of 2012 and consistently experienced severe drought conditions starting in June 2013 (figure 2; U.S. Drought Monitor 2021). Rainfall in the winter of 2016–2017 provided some drought relief, but severe drought conditions returned in 2018 (U.S. Drought Monitor 2021). Persistent rainfall from a series of atmo-

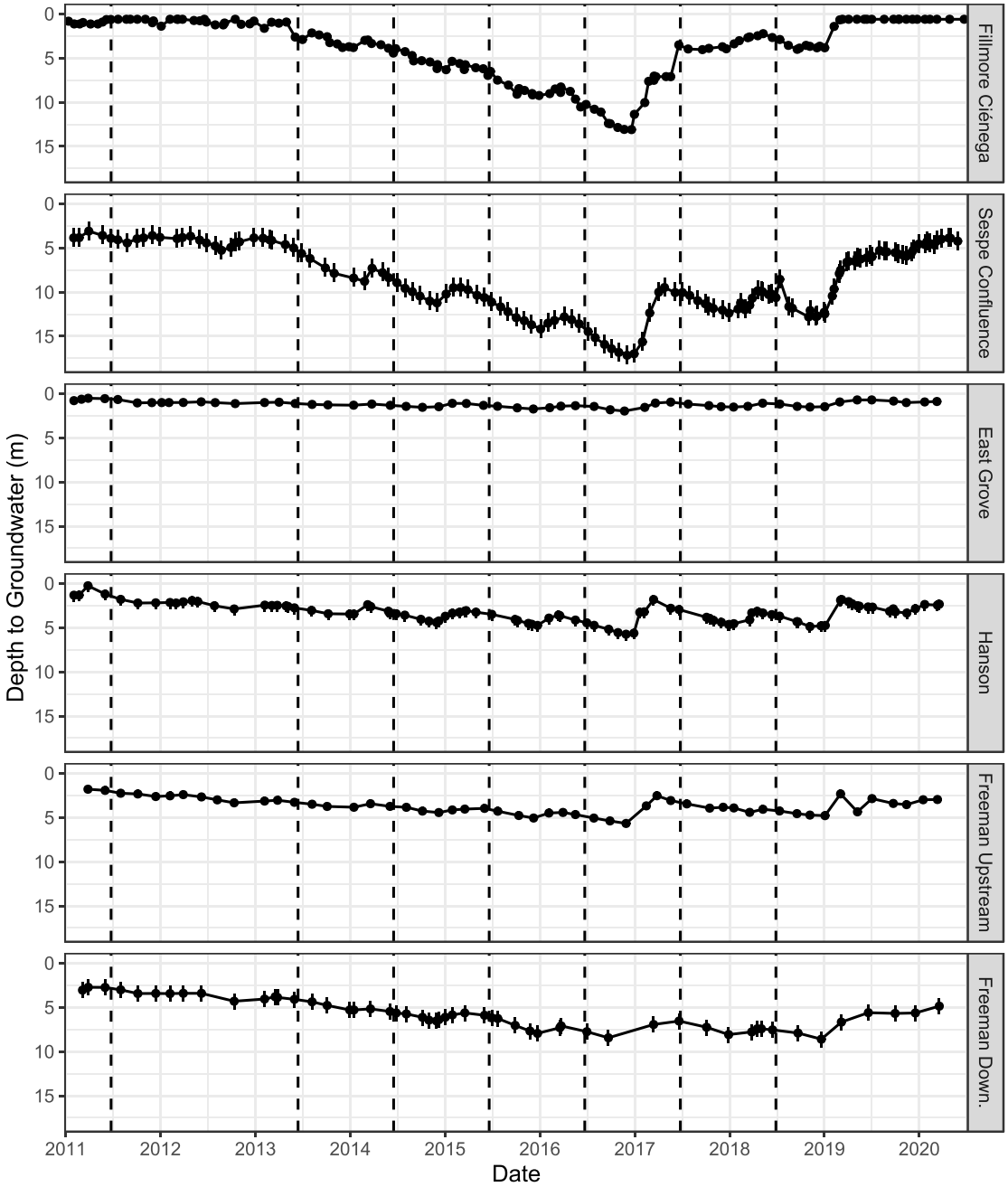

Figure 3. Mean DTG from 2011 to 2020 for each study site. The vertical bars represent the interquartile range of DTG for sites where DTG was measured by a single shallow well (see supplementary material). The dashed vertical lines indicate the remote sensing image acquisition dates. The date labels indicate 1 January of each year.

spheric rivers (Sumargo *et al* 2021) ended the drought in the winter of 2018–2019. SPEI (Vicente-Serrano *et al* 2010) values generally remained positive after February 2019, and the U.S. Drought Monitor, a composite drought index, also indicated that the drought ended in February 2019.

3.2. Groundwater level changes during and after drought

In 2011, maximum DTG at the six study sites ranged from 1.1 to 4.4 m. The DTG increased (i.e. the water table declined) at all six study sites between 2011 and 2016, but there was substantial spatial and temporal variability in DTG along the river corridor (figure 3; table S3). The changes in DTG were mediated by the interaction between climatic forcings and basin geomorphology. The Fillmore Ciénega site sits at the boundary of the Piru and Filmore groundwater subbasins (figure 1), where the deposits of permeable alluvium become substantially narrower and shallower and force groundwater to the surface (Mann Jr 1958, Reichard *et al* 1999). Surface flow between the Piru and Fillmore subbasins decreased between 2011 and 2013 and stopped between 2014 and 2016 (United Water Conservation District 2017). As a result, shallow lateral recharge of the Fillmore subbasin

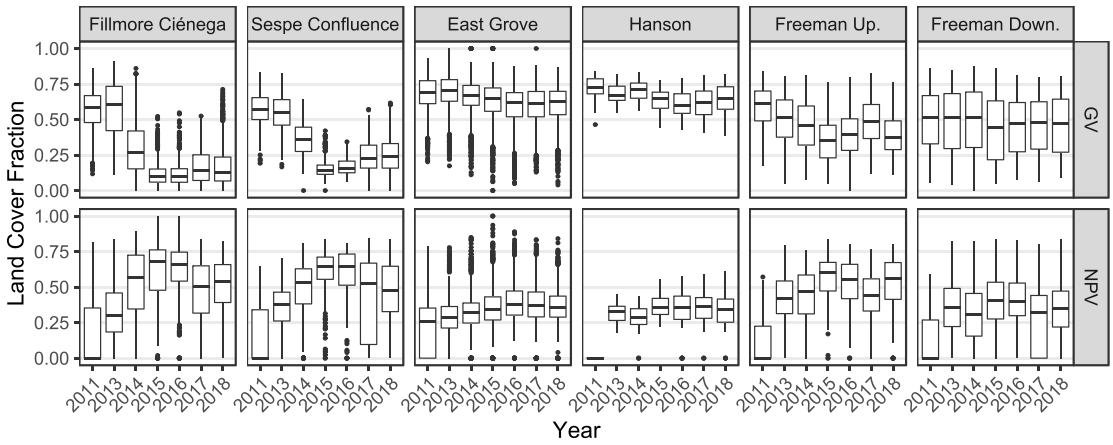

Figure 4. Box plots of green vegetation (GV) fractions and non-photosynthetic vegetation (NPV) fractions for each study site from 2011 to 2018. Note that 2012 data are omitted (see text).

was likely reduced or eliminated during the peak of the drought. Maximum DTG at Fillmore Ciénega and Sespe Confluence increased by 11.9 m and 12.7 m, respectively, between 2011 and 2016 as groundwater in the Fillmore subbasin was depleted. At the downstream end of the Fillmore subbasin, groundwater elevations were more stable. The East Grove site sits at the boundary of the Fillmore and Santa Paula subbasins, where constrictions in the deposits of unconsolidated alluvium again force groundwater to the surface (Reichard *et al* 1999). Maximum DTG at the East Grove site only increased by 0.9 m between 2011 and 2016. Surface flow at the boundary between the Fillmore and Santa Paula subbasins did not approach zero until 2016 (United Water Conservation District 2017). The Hanson, Freeman Upstream, and Freeman Downstream sites are located in the Santa Paula subbasin, where the shallow aquifer sits on top of impermeable deposits that prevent groundwater from percolating into deeper aquifers (Reichard *et al* 1999, Hanson *et al* 2003). Groundwater elevations in the Santa Paula subbasin remained relatively stable throughout the drought. At Hanson, Freeman Upstream, and Freeman Downstream, maximum DTG increased by 3.5 m, 3.0 m, and 5.0 m (respectively) between 2011 and 2016. In 2016, maximum DTG at the six sites ranged from 2.0 to 17.1 m. Substantial rainfall in the winter of 2016–2017 reversed groundwater trends and caused DTG to decrease (i.e. the water table rose) at all study sites, but some sites did not approach pre-drought DTG until 2019.

3.3. Vegetation cover change during drought

Several riparian woodlands exhibited large decreases in GV cover and large increases in NPV cover from 2011 to 2016, indicating widespread drought-induced mortality (figure 4, tables S4–S6). Fillmore Ciénega and Sespe Confluence exhibited the largest decreases in GV fractions and the largest increases in NPV fractions. Sites farther downstream were less affected by the drought and experienced smaller changes in land cover.

There was a distinct spatial pattern and temporal trend of woodland mortality that occurred both within and across study sites in the Fillmore subbasin (figure 5). Widespread mortality first occurred in 2013 at the most upstream study site, Fillmore Ciénega (figure S5). A wave of mortality then traveled 13 km west (downstream) across the Fillmore subbasin between 2013 and 2016. The wave of mortality can be seen within and across individual study sites, and it is especially distinct within the Fillmore Ciénega site. By 2015, the wave of mortality reached the area immediately upstream of the East Grove site (figure S6). By 2016, all three areas had experienced widespread mortality, and the Fillmore Ciénega and Sespe Confluence sites experienced near-complete mortality of their riparian woodlands. Sites in the downstream Santa Paula subbasin were relatively stable throughout the drought, and no distinct spatial pattern of woodland mortality in the Santa Paula subbasin was observed (figure S7).

3.4. Groundwater declines and plant health

DTG was significant predictor of the GV and NPV fractions for 2011–2016 (table 2). There was a significant negative relationship between DTG and the GV fractions ($p < 0.001$; figure 6(a)), indicating that GV decreased as the water table declined. There was also a significant positive relationship between DTG and the NPV fractions ($p < 0.001$; figure 6(b)), indicating that dead and woody plant cover increased as the water table declined. Taken together, these remote sensing metrics indicate leaf shedding, increased litter, exposed branches, and, in some cases, complete mortality as the drought progressed (Adams *et al* 1995).

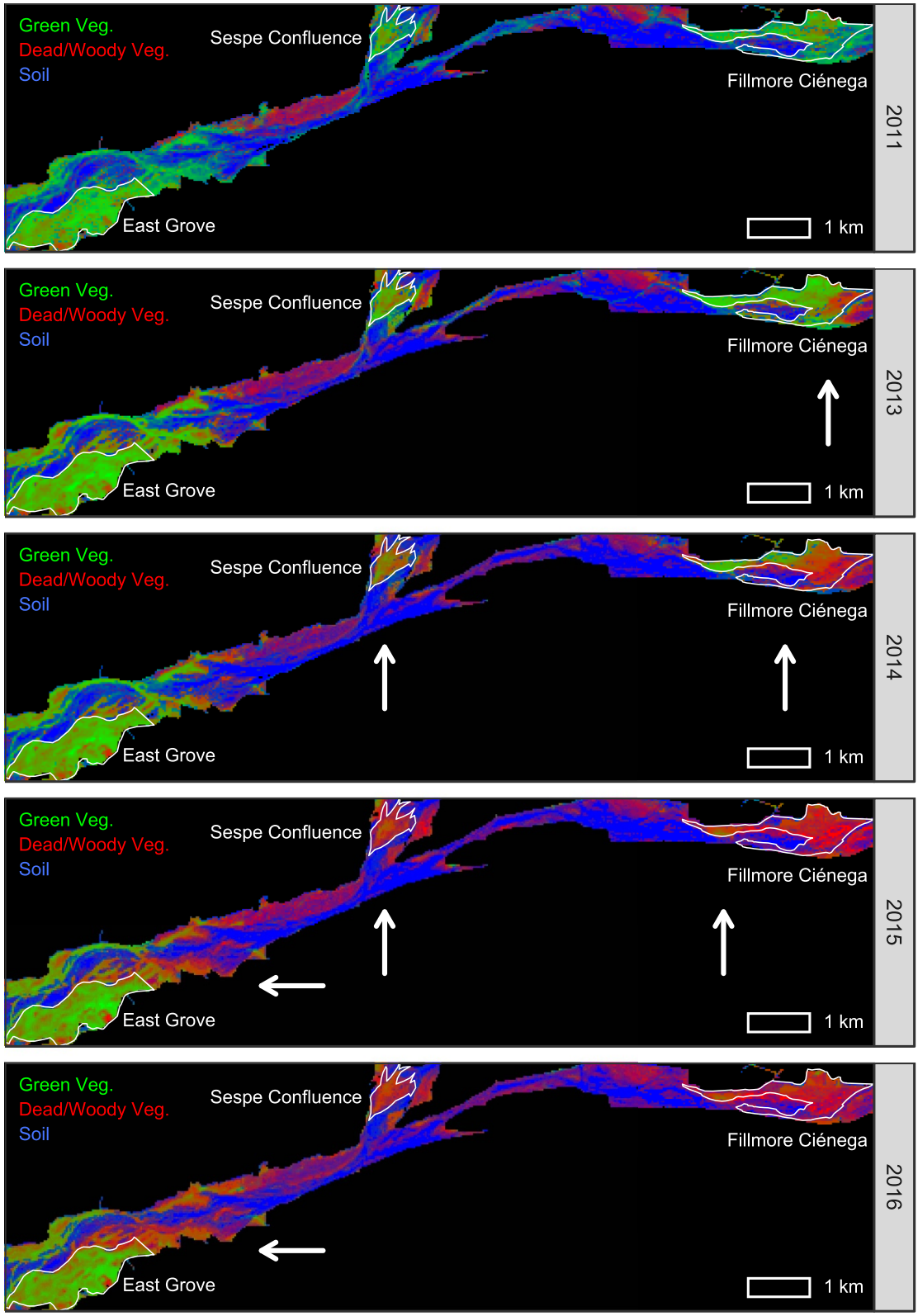

Figure 5. Remote sensing model outputs of floodplain land cover in the Fillmore subbasin from 2011 to 2016. The study sites are outlined in white, and the white arrows indicate areas experiencing notable dieback in particular years. The river flows from right to left. A comparable figure for the Hanson, Freeman Upstream, and Freeman Downstream sites is included in the supplementary material (figure S7).

3.5. Site-based differences in early drought recovery

We also compared the 2017–2018 GV fractions to the values that were predicted by the regression model, which was calibrated using data from 2011 to 2016. This revealed whether the sensitivity to DTG differed during the decline and recovery phases. The 2017–2018 GV fractions for Fillmore Ciénega deviated

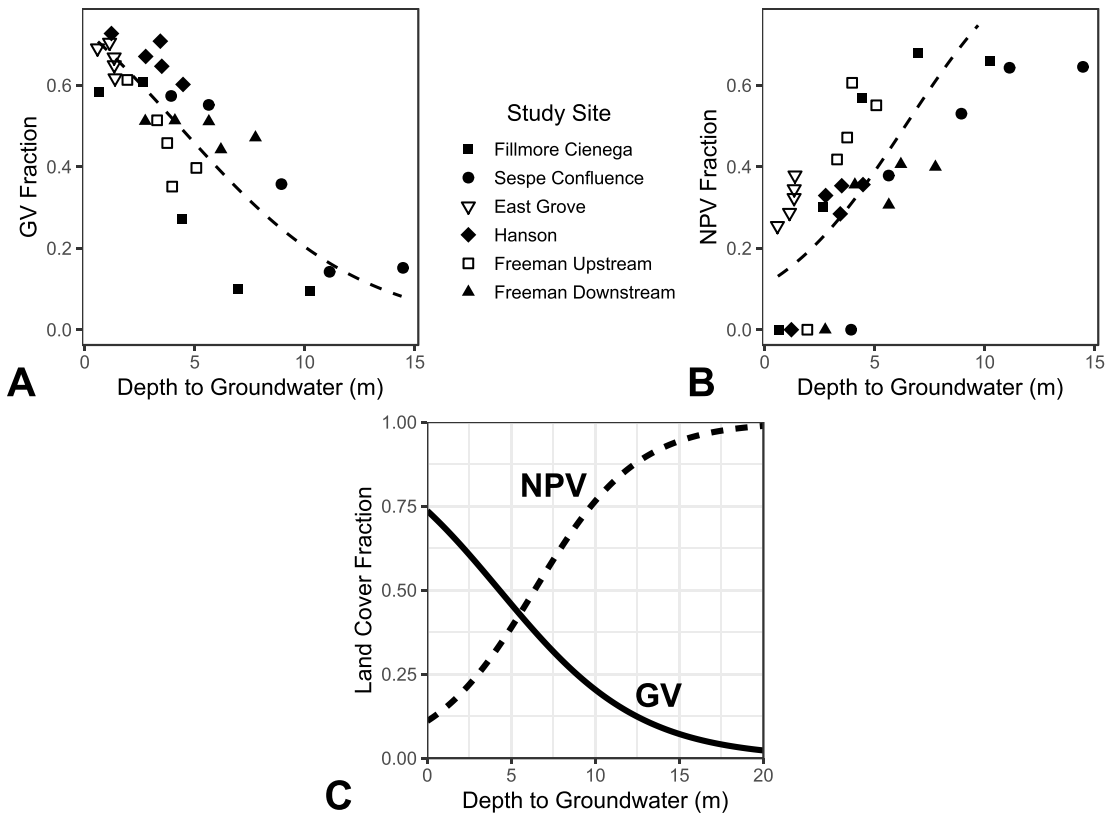

Figure 6. Scatterplots of mean DTG and median GV fractions (a) or median NPV fractions (b) from 2011 to 2016. The lines represent the modeled fixed effect of DTG on GV fractions (a), (c) and NPV fractions (b), (c).

Table 2. Mixed effect logistic-binomial regression results for models assessing the relationship between DTG and GV fractions and between DTG and NPV fractions from 2011 to 2016. Site was included as a random effect in the models. The values in parentheses indicate the standard errors of the regression coefficients.

	GV	NPV
Fixed effects		
Intercept	1.02 ***	−2.09 ***
	(0.16)	(0.28)
DTG	−0.24 ***	0.33 ***
	(0.01)	(0.01)
Random effects		
	Std. dev	Std. dev
Site (intercept)	0.38	0.68
Model		
N	30	30
N (site)	6	6
Pseudo-R^2 (fixed)	0.16	0.24
Pseudo-R^2 (total)	0.19	0.33

*** $p < 0.001$.

substantially from the values predicted by the model (decline MAE = 0.08; recovery MAE = 0.28). Fillmore Ciénega demonstrated a clear hysteresis signal, whereby groundwater rose by over 7 m (i.e. a reduced DTG), but there was only a modest increase in GV fractions (figure 7). The lack of response to rising groundwater can be explained by dead vegetation covering the site. The DTG at Sespe Confluence remained relatively deep in 2017 and 2018, and the GV fractions did not deviate substantially from the values predicted by the model (decline MAE = 0.05; recovery MAE = 0.02). The modest increase in GV fractions is likely due to the invasion of *Arundo donax* after the widespread mortality of native phreatophytes, which is a common consequence of drought conditions affecting native plants (e.g. Merritt and Poff 2010). Field observations indicate that *A. donax* now dominates the site (figure S8). The other sites, where the native woodlands remained largely intact (e.g. figure S9), exhibited consistent sensitivity to DTG during the decline (MAE = 0.02–0.07) and recovery (MAE = 0.03–0.09) phases.

4. Discussion

During the 2012–2019 California drought, riparian woodland mortality in the Santa Clara River floodplain followed a coherent spatial pattern and temporal trend that occurred across the river corridor and mirrored the apparent trend in DTG. Mortality first occurred at the upstream side of the Fillmore Ciénega site as flow between the Piru and Fillmore subbasins decreased around 2013. A distinct

'brown wave' of mortality then traveled west (i.e. upstream to downstream) between 2013 and 2016 as groundwater in the Fillmore subbasin was progressively depleted. The brown wave stopped just upstream of the East Grove site, where groundwater elevations were relatively stable and surface flow was maintained throughout most of the drought (United Water Conservation District 2017). The brown wave reveals that riparian phreatophytes are extremely sensitive to DTG over both space and time, and that localized DTG trends play an important role in determining the fate of riparian woodlands during extreme drought conditions. Few studies have quantified the sensitivity of groundwater-dependent ecosystems to DTG (e.g. Lite and Stromberg 2005), and only recently has it become possible to conduct spatially and temporally extensive analyses at a corridor scale (e.g. Huntington *et al* 2016). Such analyses were historically limited by the available remote sensing data, which were too expensive (e.g. Zhu *et al* 2019) or too coarse to resolve narrow stands of riparian woodlands (Dufour *et al* 2012). Likewise, groundwater records have only recently been aggregated and made available in comprehensive data sets.

Groundwater serves as a crucial link in the chain of drought propagation from meteorological drying to plant responses by riparian phreatophytes. The 2012–2019 California drought was caused by record low precipitation and record high temperatures, which reduced water inputs to ecosystems and increased evaporative demand (Diffenbaugh *et al* 2015, Warter *et al* 2021). The drought generally reduced groundwater recharge (Harlow and Hagedorn 2018) and caused groundwater elevations to decline, but subsurface water fluxes are spatially variable and are mediated by several factors including agricultural water use and runoff, river regulation, soil texture, and bedrock geology. During drought conditions, the hydrological drivers of groundwater elevation interact with meteorological trends to produce distinct spatial patterns and temporal trends of groundwater change (Jencso and McGlynn 2011, Harlow and Hagedorn 2018).

The spatiotemporal variability in groundwater elevation caused varying physiological responses in the riparian woodlands in the Santa Clara River floodplain. When water tables decline by several meters, the root systems of riparian trees can lose access to groundwater (Stromberg 2013). Riparian tree species are poorly adapted to drought and can experience catastrophic xylem cavitation at relatively high (i.e. close to zero) vapor pressure deficits (Fichot *et al* 2015). To mitigate and prevent this often-irreversible change, trees undergo a series of physiological changes to maintain a favorable water balance in the face of declining water supply (Rood *et al* 2003). Within minutes, they can regulate stomatal conductance to limit transpirational water loss (Horton *et al* 2001, Amlin and Rood 2003, Pivovaroff *et al* 2018). Leaf abscission and branch dieback, though detrimental to woody plants in the short term, can serve as long-term survival strategies that help trees reduce water demand and prevent the loss of xylem water conductance (Scott *et al* 1999, Rood *et al* 2000, Cooper *et al* 2003). These physiological responses may not be adequate to mitigate water stress from large and sudden water table declines, which often cause hydraulic failure and whole-plant mortality (Scott *et al* 1999, Lite and Stromberg 2005, Tai *et al* 2018).

The brown wave is likely an emergent property of individual plants responding to localized changes in DTG, as evidenced by the fine-scale changes in plant health and the strong statistical relationships between the land cover fractions and DTG. Few studies have examined the spatial evolution of riparian woodland responses to water table declines (but see Stromberg *et al* 1996, Scott *et al* 1999, 2000, Tai *et al* 2018). The current understanding of phreatophyte sensitivity to DTG is largely derived from field measurements (e.g. Horton *et al* 2001, Rood *et al* 2011), laboratory experiments (e.g. Leffler *et al* 2000, Stella *et al* 2010), and models based on phreatophyte physiology (e.g. Tai *et al* 2018). These data have resulted in a conceptual model that suggests that there is a highly non-linear relationship between DTG and plant health, whereby plant health degrades rapidly when DTG increases beyond some critical threshold (e.g. Shafroth *et al* 2000, Horton *et al* 2001, Lite and Stromberg 2005). In contrast with previous studies, our observations indicate that there is a mostly linear relationship between DTG and plant health at a stand scale when DTG is less than 10 m (i.e. figure 6(c)). The difference in the shape of the observed relationships may indicate a scale dependence of the analysis. While many field and laboratory-based studies examine individual plants belonging to selected species, remote sensing data detects many plants belonging to many species within a pixel (Kibler *et al* 2019). The observed plants that compose riparian woodlands likely have varying structures, life histories, and tolerances for groundwater decline (Stromberg *et al* 1996, Stromberg and Merritt 2016). Nonetheless, the observed sensitivity to absolute DTG and DTG change (table S3) were generally consistent with previously reported values. At Fillmore Ciénega and Sespe Confluence, vegetation cover stopped changing as a function of DTG between 2015 and 2016, which may indicate a fundamental limit beyond which phreatophytes experience complete mortality and the health of the surviving non-phreatophytic vegetation becomes decoupled from DTG. The recovery of phreatophytes at these sites depends on the water table returning to shallow depths and seed sources for the germination of new seedlings (Stella *et al* 2006).

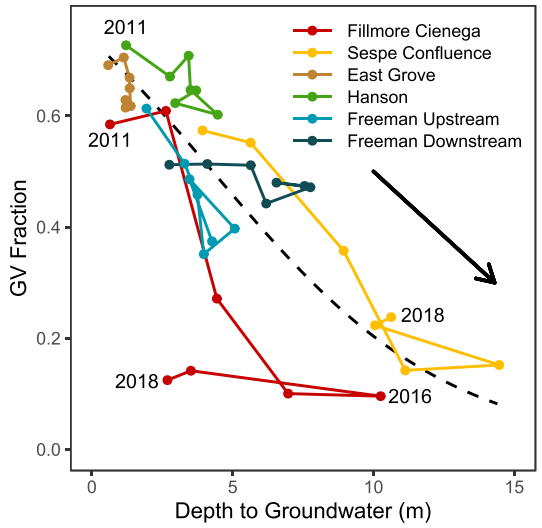

Figure 7. Scatterplot of DTG and median GV fractions from 2011 to 2018. The line segments connect observations from consecutive years. The observations from 2011 are generally in the upper left and the observations from 2018 are generally in the lower right. Observations from 2012 are omitted (see text). The dashed line represents the modeled fixed effect of DTG on GV fractions for data from 2011 to 2016.

5. Conclusion

The statistical analyses presented here provide some of the first robust estimates of the sensitivity of riparian woodlands to DTG. Our findings also reveal that DTG trends can be highly variable during extreme drought conditions, even within the same river corridor, which can result in distinct spatial patterns and temporal trends of plant mortality in riparian woodlands. Quantifying the sensitivity of riparian ecosystems to groundwater change will become increasingly important as anthropogenic climate change increases the frequency and severity of drought conditions across the western United States (Diffenbaugh *et al* 2015, Rohde *et al* 2017, Williams *et al* 2020). The widespread mortality observed during the brown wave mirrors the dynamics of mass die-offs that have occurred in upland forest ecosystems (e.g. Allen *et al* 2010, Goulden and Bales 2019). Anthropogenic climate change, shifts in water availability, and other environmental forcings are overwhelming the resiliency of ecosystems that are typically buffered from climatic variability (Allen *et al* 2015). Quantifying the sensitivity of both upland and lowland forests to hydroclimatic change will improve our ability to predict critical shifts in ecosystem structure and function in the coming decades.

Data availability statement

The data that support the findings of this study are available upon reasonable request from the authors.

Acknowledgments

The authors thank Jared Williams, Sean Carey, Margot Mason, Peter Downs, and David Miller for their assistance with this study. We also thank the Nature Conservancy for providing access to their properties. Support for this work came from the U.S. National Science Foundation (BCS-1660490, EAR-1700555, and EAR-1700517) and the U.S. Department of Defense's Strategic Environmental Research and Development Program (RC18-1006).

ORCID iDs

Christopher L Kibler https://orcid.org/0000-0002-3260-0188
Dar A Roberts https://orcid.org/0000-0002-3555-4842
John C Stella https://orcid.org/0000-0001-6095-7726
Li Kui https://orcid.org/0000-0002-5894-4907
Adam M Lambert https://orcid.org/0000-0001-7035-1787
Michael Bliss Singer https://orcid.org/0000-0002-6899-2224

References

Abatzoglou J T 2013 Development of gridded surface meteorological data for ecological applications and modelling *Int. J. Climatol.* **33** 121–31
Adams J B, Sabol D E, Kapos V, Filho R A, Roberts D A, Smith M O and Gillespie A R 1995 Classification of multispectral images based on fractions of endmembers: application to land-cover change in the Brazilian Amazon *Remote Sens. Environ.* **52** 137–54
Allen C D *et al* 2010 A global overview of drought and heat-induced tree mortality reveals emerging climate change risks for forests *For. Ecol. Manage.* **259** 660–84
Allen C D, Breshears D D and McDowell N G 2015 On underestimation of global vulnerability to tree mortality and forest die-off from hotter drought in the Anthropocene *Ecosphere* **6** art129
Amlin N M and Rood S B 2003 Drought stress and recovery of riparian cottonwoods due to water table alteration along Willow Creek, Alberta *Trees* **17** 351–8
Anderegg W R L, Kane J M and Anderegg L D L 2013 Consequences of widespread tree mortality triggered by drought and temperature stress *Nat. Clim. Change* **3** 30–36
Andersen T, Carstensen J, Hernández-García E and Duarte C M 2009 Ecological thresholds and regime shifts: approaches to identification *Trends Ecol. Evol.* **24** 49–57
Asner G P, Brodrick P G, Anderson C B, Vaughn N, Knapp D E and Martin R E 2016 Progressive forest canopy water loss during the 2012–2015 California drought *Proc. Natl Acad. Sci.* **113** E249–55
Barron O V, Emelyanova I, van Niel T G, Pollock D and Hodgson G 2014 Mapping groundwater-dependent ecosystems using remote sensing measures of vegetation and moisture dynamics *Hydrol. Process.* **28** 372–85
Bateman H L and Merritt D M 2020 Complex riparian habitats predict reptile and amphibian diversity *Glob. Ecol. Conserv.* **22** e00957
Beisner B, Haydon D and Cuddington K 2003 Alternative stable states in ecology *Front. Ecol. Environ.* **1** 376–82

Beller E E, Downs P W, Grossinger R M, Orr B K and Salomon M N 2016 From past patterns to future potential: using historical ecology to inform river restoration on an intermittent California river *Landsc. Ecol.* **31** 581–600

Brooks P D, Chorover J, Fan Y, Godsey S E, Maxwell R M, McNamara J P and Tague C 2015 Hydrological partitioning in the critical zone: recent advances and opportunities for developing transferable understanding of water cycle dynamics *Water Resour. Res.* **51** 6973–87

Cooper D J, d'Amico D R and Scott M L 2003 Physiological and morphological response patterns of *Populus deltoides* to alluvial groundwater pumping *Environ. Manage.* **31** 215–26

Diffenbaugh N S, Swain D L and Touma D 2015 Anthropogenic warming has increased drought risk in California *Proc. Natl Acad. Sci.* **112** 3931–6

Dong C, MacDonald G M, Willis K, Gillespie T W, Okin G S and Williams A P 2019 Vegetation responses to 2012–2016 drought in northern and southern California *Geophys. Res. Lett.* **46** 3810–21

Downs P W, Dusterhoff S R and Sears W A 2013 Reach-scale channel sensitivity to multiple human activities and natural events: Lower Santa Clara River, California, USA *Geomorphology* **189** 121–34

Dufour S, Muller E, Straatsma M and Corgne S 2012 Image utilisation for the study and management of riparian vegetation: overview and applications *Fluvial Remote Sensing for Science and Management* ed P Carbonneau and H Piégay (Chichester: Wiley-Blackwell) 215–39

Dybala K E, Matzek V, Gardali T and Seavy N E 2019 Carbon sequestration in riparian forests: a global synthesis and meta-analysis *Glob. Change Biol.* **25** 57–67

Fichot R, Brignolas F, Cochard H and Ceulemans R 2015 Vulnerability to drought-induced cavitation in poplars: synthesis and future opportunities: drought-induced cavitation in poplars: a review *Plant Cell Environ.* **38** 1233–51

Gary H L 1963 Root distribution of five-stamen tamarisk, seepwillow, and arrowweed *For. Sci.* **9** 311–4

Gelman A and Hill J 2007 *Data Analysis Using Regression and Multilevel/hierarchical Models* (Cambridge: Cambridge University Press)

Goulden M L and Bales R C 2019 California forest die-off linked to multi-year deep soil drying in 2012–2015 drought *Nat. Geosci.* **12** 632–7

Green R O *et al* 1998 Imaging spectroscopy and the airborne visible/infrared imaging spectrometer (AVIRIS) *Remote Sens. Environ.* **65** 227–48

Hanson R T, Martin P and Koczot K M 2003 *Simulation of Ground-Water/Surface-Water Flow in the Santa Clara–Calleguas Ground-Water Basin, Ventura County, California* Water-Resources Investigations Report No. 02-4136 U.S. Geological Survey p 157 (available at: https://pubs.usgs.gov/wri/wri024136/text.html)

Harlow J and Hagedorn B 2018 SWB modeling of groundwater recharge on Catalina Island, California, during a period of severe drought *Water* **11** 58

Horton J L, Kolb T E and Hart S C 2001 Responses of riparian trees to interannual variation in ground water depth in a semi-arid river basin *Plant Cell Environ.* **24** 293–304

Hoylman Z H, Jencso K G, Hu J, Holden Z A, Allred B, Dobrowski S, Robinson N, Martin J T, Affleck D and Seielstad C 2019 The topographic signature of ecosystem climate sensitivity in the western United States *Geophys. Res. Lett.* **46** 14508–20

Huang C, Anderegg W R L and Asner G P 2019 Remote sensing of forest die-off in the Anthropocene: from plant ecophysiology to canopy structure *Remote Sens. Environ.* **231** 111233

Huntington J L, Hegewisch K C, Daudert B, Morton C G, Abatzoglou J T, McEvoy D J and Erickson T 2017 Climate engine: cloud computing and visualization of climate and remote sensing data for advanced natural resource monitoring and process understanding *Bull. Am. Meteorol. Soc.* **98** 2397–410

Huntington J, McGwire K, Morton C, Snyder K, Peterson S, Erickson T, Niswonger R, Carroll R, Smith G and Allen R 2016 Assessing the role of climate and resource management on groundwater dependent ecosystem changes in arid environments with the Landsat archive *Remote Sens. Environ.* **185** 186–97

Jencso K G and McGlynn B L 2011 Hierarchical controls on runoff generation: topographically driven hydrologic connectivity, geology, and vegetation *Water Resour. Res.* **47** 11

Kibler C L, Parkinson A-M L, Peterson S H, Roberts D A, d'Antonio C M, Meerdink S K and Sweeney S H 2019 Monitoring post-fire recovery of chaparral and conifer species using field surveys and Landsat time series *Remote Sens.* **11** 2963

Konrad C P 2019 Seasonal precipitation influences streamflow vulnerability to the 2015 drought in the western United States *J. Hydrometeorol.* **20** 1261–74

Kovach R P *et al* 2019 An integrated framework for ecological drought across riverscapes of North America *BioScience* **69** 418–31

Kus B E 1998 Use of restored riparian habitat by the endangered Least Bell's Vireo (*Vireo bellii pusillus*) *Restor. Ecol.* **6** 75–82

Leffler A J, England L E and Naito J 2000 Vulnerability of Fremont cottonwood (*Populus fremontii* Wats.) individuals to xylem cavitation *West. N. Am. Nat.* **60** 204–10

Lite S J and Stromberg J C 2005 Surface water and ground-water thresholds for maintaining Populus–Salix forests, San Pedro River, Arizona *Biol. Conserv.* **125** 153–67

Mahoney J M and Rood S B 1998 Streamflow requirements for cottonwood seedling recruitment—an integrative model *Wetlands* **18** 634–45

Mann Jr J F 1958 *Preliminary Outline of Groundwater Conditions Near State Fish Hatchery* Memo to United Water Conservation District

Markham B L, Storey J C, Williams D L and Irons J R 2004 Landsat sensor performance: history and current status *IEEE Trans. Geosci. Remote Sens.* **42** 2691–4

Matzek V, Stella J, Ropion P and Marrs R 2018 Development of a carbon calculator tool for riparian forest restoration *Appl. Veg. Sci.* **21** 584–94

McDowell N G *et al* 2016 Multi-scale predictions of massive conifer mortality due to chronic temperature rise *Nat. Clim. Change* **6** 295–300

Meixner T *et al* 2016 Implications of projected climate change for groundwater recharge in the western United States *J. Hydrol.* **534** 124–38

Merritt D M and Bateman H L 2012 Linking stream flow and groundwater to avian habitat in a desert riparian system *Ecol. Appl.* **22** 1973–88

Merritt D M and Poff N L R 2010 Shifting dominance of riparian *Populus* and *Tamarix* along gradients of flow alteration in western North American rivers *Ecol. Appl.* **20** 135–52

Munson S M, Bradford J B and Hultine K R 2020 An integrative ecological drought framework to span plant stress to ecosystem transformation *Ecosystems* **24** 739–54

Okin G S, Dong C, Willis K S, Gillespie T W and MacDonald G M 2018 The impact of drought on native southern California vegetation: remote sensing analysis using MODIS-derived time series *J. Geophys. Res. Biogeosci.* **123** 1927–39

Pettit N E and Froend R H 2018 How important is groundwater availability and stream perenniality to riparian and floodplain tree growth? *Hydrol. Process.* **32** 1502–14

Pivovaroff A L, Cook V M W and Santiago L S 2018 Stomatal behaviour and stem xylem traits are coordinated for woody plant species under exceptional drought conditions: xylem and stomata under extreme drought *Plant Cell Environ.* **41** 2617–26

Rateb A *et al* 2020 Comparison of groundwater storage changes from GRACE satellites with monitoring and modeling of major U.S. aquifers *Water Resour. Res.* **56** 12

Reichard E G, Crawford S M, Paybins K S, Martin P, Land M and Nishikawa T 1999 *Evaluation of Surface-Water/Ground-Water Interactions in the Santa Clara River Valley, Ventura County, California* Water-Resources Investigations Report No. 98-4208 U.S. Geological Survey p 58 (available at: https://pubs.er.usgs.gov/publication/wri984208)

Roberts D A, Gardner M, Church R, Ustin S, Scheer G and Green R O 1998 Mapping chaparral in the Santa Monica Mountains using multiple endmember spectral mixture models *Remote Sens. Environ.* **65** 267–79

Robeson S M 2015 Revisiting the recent California drought as an extreme value *Geophys. Res. Lett.* **42** 6771–9

Rohde M M, Froend R and Howard J 2017 A global synthesis of managing groundwater dependent ecosystems under sustainable groundwater policy *Groundwater* **55** 293–301

Rohde M M, Stella J C, Roberts D A and Singer M B 2021 Groundwater dependence of riparian woodlands and the disrupting effect of anthropogenically altered streamflow *Proc. Natl Acad. Sci.* **118** e2026453118

Rood S B, Bigelow S G and Hall A A 2011 Root architecture of riparian trees: river cut-banks provide natural hydraulic excavation, revealing that cottonwoods are facultative phreatophytes *Trees* **25** 907–17

Rood S B, Braatne J H and Hughes F M R 2003 Ecophysiology of riparian cottonwoods: stream flow dependency, water relations and restoration *Tree Physiol.* **23** 1113–24

Rood S B, Patiño S, Coombs K and Tyree M T 2000 Branch sacrifice: cavitation-associated drought adaptation of riparian cottonwoods *Trees* **14** 0248–57

Sargeant C I and Singer M B 2016 Sub-annual variability in historical water source use by Mediterranean riparian trees: sub-annual riparian tree water use *Ecohydrology* **9** 1328–45

Scott M L, Lines G C and Auble G T 2000 Channel incision and patterns of cottonwood stress and mortality along the Mojave River, California *J. Arid Environ.* **44** 399–414

Scott M L, Shafroth P B and Auble G T 1999 Responses of riparian cottonwoods to alluvial water table declines *Environ. Manage.* **23** 347–58

Shafroth P B, Stromberg J C and Patten D T 2000 Woody riparian vegetation response to different alluvial water table regimes *West. N. Am. Nat.* **60** 66–76

Singer M B, Sargeant C I, Piégay H, Riquier J, Wilson R J S and Evans C M 2014 Floodplain ecohydrology: climatic, anthropogenic, and local physical controls on partitioning of water sources to riparian trees *Water Resour. Res.* **50** 4490–513

Singer M B, Stella J C, Dufour S, Piégay H, Wilson R J S and Johnstone L 2013 Contrasting water-uptake and growth responses to drought in co-occurring riparian tree species *Ecohydrology* **6** 402–12

Skiadaresis G, Schwarz J, Stahl K and Bauhus J 2021 Groundwater extraction reduces tree vitality, growth and xylem hydraulic capacity in *Quercus robur* during and after drought events *Sci. Rep.* **11** 5149

Smith M O, Ustin S L, Adams J B and Gillespie A R 1990 Vegetation in deserts: I. A regional measure of abundance from multispectral images *Remote Sens. Environ.* **31** 1–26

Stella J C and Battles J J 2010 How do riparian woody seedlings survive seasonal drought? *Oecologia* **164** 579–90

Stella J C, Battles J J, McBride J R and Orr B K 2010 Riparian seedling mortality from simulated water table recession, and the design of sustainable flow regimes on regulated rivers *Restor. Ecol.* **18** 284–94

Stella J C, Battles J J, Orr B K and McBride J R 2006 Synchrony of seed dispersal, hydrology and local climate in a semi-arid river reach in California *Ecosystems* **9** 1200–14

Stover J, Keller E, Dudley T and Langendoen E 2018 Fluvial geomorphology, root distribution, and tensile strength of the invasive giant reed, *Arundo donax* and its role on stream bank stability in the Santa Clara River, southern California *Geosciences* **8** 304

Stromberg J C 2013 Root patterns and hydrogeomorphic niches of riparian plants in the American Southwest *J. Arid Environ.* **94** 1–9

Stromberg J C and Merritt D M 2016 Riparian plant guilds of ephemeral, intermittent and perennial rivers *Freshw. Biol.* **61** 1259–75

Stromberg J C, Tiller R and Richter B 1996 Effects of groundwater decline on riparian vegetation of semiarid regions: the San Pedro, Arizona *Ecol. Appl.* **6** 113–31

Sumargo E, McMillan H, Weihs R, Ellis C J, Wilson A M and Ralph F M 2021 A soil moisture monitoring network to assess controls on runoff generation during atmospheric river events *Hydrol. Process.* **35** 1

Swetnam T L, Brooks P D, Barnard H R, Harpold A A and Gallo E L 2017 Topographically driven differences in energy and water constrain climatic control on forest carbon sequestration *Ecosphere* **8** e01797

Tai X, Mackay D S, Sperry J S, Brooks P, Anderegg W R L, Flanagan L B, Rood S B and Hopkinson C 2018 Distributed plant hydraulic and hydrological modeling to understand the susceptibility of riparian woodland trees to drought-induced mortality *Water Resour. Res.* **54** 4901–15

Taylor R G *et al* 2013 Ground water and climate change *Nat. Clim. Change* **3** 322–9

The Nature Conservancy 2021 Groundwater Resource Hub *Plant Rooting Depth Database* (available at: https://groundwaterresourcehub.org/sgma-tools/gde-rooting-depths-database-for-gdes/) (Accessed 8 April 2021)

Thomas B F, Famiglietti J S, Landerer F W, Wiese D N, Molotch N P and Argus D F 2017 GRACE groundwater drought index: evaluation of California Central Valley groundwater drought *Remote Sens. Environ.* **198** 384–92

U.S. Department of Agriculture 2012 National Agricultural Imagery Program *Aerial Imagery of the Santa Clara River Watershed* (available at: https://nrcs.app.box.com/v/naip/folder/17936490251) (Retrieved 8 April 2021)

U.S. Department of Agriculture 2021 The PLANTS database National Plant Data Team, Greensboro, NC (available at: https://plants.sc.egov.usda.gov/java) (Accessed 8 April 2021)

U.S. Drought Monitor 2021 Time series for the Santa Clara River watershed (available at: https://droughtmonitor.unl.edu) (Accessed 8 April 2021)

United Water Conservation District 2017 *Groundwater and Surface Water Conditions Report—2015* Open-File Report No. 2017-01 p 198 (available at: www.unitedwater.org/key-documents/#groundwater-conditions)

van Loon A F 2015 Hydrological drought explained *Wiley Interdiscip. Rev. Water* **2** 359–92

Vicente-Serrano S M, Beguería S and López-Moreno J I 2010 A multiscalar drought index sensitive to global warming: the standardized precipitation evapotranspiration index *J. Clim.* **23** 1696–718

Warter M M, Singer M B, Cuthbert M O, Roberts D, Caylor K K, Sabathier R and Stella J 2021 Drought onset and propagation into soil moisture and grassland vegetation responses during the 2012–2019 major drought in Southern California *Hydrol. Earth Syst. Sci.* **25** 3713–29

Williams A P, Cook E R, Smerdon J E, Cook B I, Abatzoglou J T, Bolles K, Baek S H, Badger A M and Livneh B 2020 Large contribution from anthropogenic warming to an emerging North American megadrought *Science* **368** 314–8

Zhu Z *et al* 2019 Benefits of the free and open Landsat data policy *Remote Sens. Environ.* **224** 382–5

Zimmerman R C 1969 *Plant Ecology of an Arid Basin: Tres Alamos-Redington Area, Southeastern Arizona* Geological Survey Professional Paper No. 485-D U.S. Department of the Interior (available at: https://pubs.usgs.gov/pp/0485d/report.pdf)